

**This is an electronic reprint of the original article.
This reprint *may differ* from the original in pagination and typographic detail.**

Author(s): Närhi, Sari; Kutuniva, Johanna; Lajunen, Marja; Lahtinen, Manu; Tuononen, Heikki;
Karttunen, Antti; Oilunkaniemi, Raija; Laitinen, Risto

Title: Identification of mixed bromidochloridotellurate anions in disordered crystal structures of $(\text{bdmim})_2[\text{TeX}_2\text{Y}_4]$ (X, Y = Br, Cl; bdmim = 1-butyl-2,3-dimethylimidazolium) by combined application of Raman spectroscopy and solid-state DFT calculations
Year: 2014

Version:

Please cite the original version:

Närhi, S., Kutuniva, J., Lajunen, M., Lahtinen, M., Tuononen, H., Karttunen, A., Oilunkaniemi, R., & Laitinen, R. (2014). Identification of mixed bromidochloridotellurate anions in disordered crystal structures of $(\text{bdmim})_2[\text{TeX}_2\text{Y}_4]$ (X, Y = Br, Cl; bdmim = 1-butyl-2,3-dimethylimidazolium) by combined application of Raman spectroscopy and solid-state DFT calculations. *Spectrochimica Acta Part A: Molecular and Biomolecular Spectroscopy*, 117, 728-738. <https://doi.org/10.1016/j.saa.2013.09.063>

All material supplied via JYX is protected by copyright and other intellectual property rights, and duplication or sale of all or part of any of the repository collections is not permitted, except that material may be duplicated by you for your research use or educational purposes in electronic or print form. You must obtain permission for any other use. Electronic or print copies may not be offered, whether for sale or otherwise to anyone who is not an authorised user.

Identification of Mixed Bromidochloridotellurate Anions in Disordered Crystal Structures of (bdmim)₂[TeX₂Y₄] (X, Y = Br, Cl; bdmim = 1-butyl-2,3-dimethylimidazolium) by Combined Application of Raman Spectroscopy and Solid-state DFT Calculations

Sari M. Närhi,^a Johanna Kutuniva,^a Marja K. Lajunen,^a Manu K. Lahtinen,^b Heikki M. Tuononen,^b Antti J. Karttunen,^b Raija Oilunkaniemi,^{*,a} and Risto S. Laitinen,^{*,a}

[a] Department of Chemistry, University of Oulu, P.O. Box 3000, FI-90014 Oulu, Finland.

E-mail: raija.oilunkaniemi@oulu.fi, risto.laitinen@oulu.fi

[b] Department of Chemistry, University of Jyväskylä, P.O. Box 35, FI-40014 Jyväskylä, Finland.

Abstract

The discrete mixed $[\text{TeBr}_x\text{Cl}_{6-x}]^{2-}$ anions in their disordered crystal structures have been identified by using the phases prepared by the reaction of 1-butyl-2,3-dimethylimidazolium halogenides (bdmim)X with tellurium tetrahalogenides TeX_4 ($X = \text{Cl}, \text{Br}$) as examples. Homoleptic (bdmim) $_2$ $[\text{TeX}_6]$ [$X = \text{Cl}$ (**1**), Br (**2**)] and mixed (bdmim) $_2$ $[\text{TeBr}_2\text{Cl}_4]$ (**3**), and (bdmim) $_2$ $[\text{TeBr}_4\text{Cl}_2]$ (**4**) are formed depending on the choice of the reagents, and their crystal structures have been determined by single-crystal X-ray diffraction. The coordination environments of tellurium in all hexahalogenidotellurates are almost octahedral. Because of the crystallographic disorder, the mixed $[\text{TeBr}_2\text{Cl}_4]^{2-}$ and $[\text{TeBr}_4\text{Cl}_2]^{2-}$ anions in **3** and **4** cannot be identified in their crystal structures. Pawley refinement of the X-ray powder diffraction patterns of **1-4** indicates the presence of single phases in all four products. The solid state Raman spectra of **1-4** were assigned with help of DFT calculations that were performed both for the discrete anions in vacuum and for the complete crystal structures employing periodic boundary conditions. The fundamental vibrations of the homoleptic $[\text{TeX}_6]^{2-}$ ($X = \text{Cl}, \text{Br}$) anions could be well reproduced by the solid-state DFT computations and enabled a complete assignment of the Raman spectra. While the presence of *cis*-isomers in both $[\text{TeBr}_2\text{Cl}_4]^{2-}$ and $[\text{TeBr}_4\text{Cl}_2]^{2-}$ could be inferred by the computed fundamental vibrations, that of *trans*-isomers among the reaction product is, however, also possible. The pathway of the formation of $[\text{TeX}_4\text{Y}_2]^{2-}$ isomers from TeX_4 and Y^- ($X, Y = \text{Cl}, \text{Br}$) was also explored by DFT calculations both in vacuum and in solution and indicated that both reactions afforded 80 mol % of *cis*-isomers and 20 mol % of *trans*-isomers.

1. Introduction.

X-ray crystallography provides the most definite means to elucidate structures of different types of materials at the molecular level. However, successful routine structure determinations require crystalline material, which contains well-defined single crystals with ordered, periodically repeating structures. In many cases this is not a case. For instance, disorder and twinning are common occurrences, and the number of modular structures is continually growing. Various techniques have been developed to deal with some of these problems, as exemplified in refs. 1-5, though some types of disorder cannot be resolved by X-ray crystallography alone.

Spectroscopic methods have often been evoked to resolve the crystallographic disorder. For instance, crystalline eight-membered $\text{Se}_n\text{S}_{8-n}$ ring molecules [6] or $[\text{TiCp}_2\text{Se}_n\text{S}_{5-n}]$ complexes [7] are solid solutions of 30 and 20 molecular species, respectively, taking the presence of isomers into account. Consequently, each chalcogen-atom sites in both compounds are partially occupied by sulfur and selenium atoms. In both cases, individual molecules have been identified by dissolving the crystalline samples, and recording and assigning their ^{77}Se NMR spectra [6, 7].

Vibrational spectroscopy is useful in the identification of individual species in disordered crystal structures, as exemplified by the characterization of $\text{RbH}(\text{SO}_4)_{0.81}(\text{SeO}_4)_{0.19}$ [8], 1,2,3- Se_3S_5 [9], and 1,5- $\text{Se}_2\text{S}_2\text{N}_4$ [10], which are pure stoichiometric species or nearly so but which show orientational disorder in the lattices. The interpretation of the vibrational spectra has often been based on force-field calculations, but with the increase of computational efficiency the spectral assignment has also been carried out by calculating fundamental vibrations with ab initio or DFT MO methods in the gaseous state or solution (for some examples, see ref. 11-14). The introduction of periodic boundary conditions for ab initio and DFT calculations has facilitated

modeling of crystal structures in the solid state [15-17]. The method has recently also proven powerful for the computation of fundamental vibrations [15, 18, 19].

While sufficiently high-level ab initio and DFT computations for the molecular species in the gas-state or solution yield fundamental vibrations, which show close enough an agreement to those observed in the IR or Raman spectra of the solid crystalline materials, the situation is not so straight-forward for ionic substances containing polyatomic cations and anions. In the gas state the multiply-charged polyatomic ions suffer from so called electronic instability [20] and consequently the calculated wavenumbers in the gas state or solution show systematically too low values. The electronic instability refers to inappropriately high orbital energies in discrete negatively charged species in absence of anion-cation interactions. The HOMO orbitals may even show positive values. At the worst case it is not possible to carry out the assignment of the observed vibrational spectra. Solid-state DFT calculations with periodic boundary conditions, which take ion-pair interactions into account, circumvent this problem and provide a promising approach to characterize ionic disordered structures. Not only is the agreement between the observed and calculated wavenumbers better, but the solid-state computations also take into account the lower site symmetry in crystals compared to idealized geometries in vacuum.

Salts of the $[\text{TeBr}_x\text{Cl}_{6-x}]^{2-}$ ($x = 0-6$) anions constitute a good system to explore the suitability of solid-state DFT methods to calculate the vibrational spectra of compounds of polyatomic ions. A large number of salts containing homoleptic $[\text{TeX}_6]^{2-}$ ($X = \text{Cl}, \text{Br}$) anions with different counterions have been prepared and structurally characterized [21]. Their structures and vibrational spectroscopic properties are well-known and they serve as benchmarks to establish the level of reliability in the current DFT methods in identification and spectroscopic characterization. By contrast, the information of mixed $[\text{TeCl}_x\text{Br}_{6-x}]^{2-}$ anions is much sparser

describing mainly the preparation of the salts [21-31]. Only a few crystal structure determinations are known. $\text{Rb}_2\text{TeBr}_{3.5}\text{Cl}_{2.5}$ has been reported to contain a disordered mixture of $[\text{TeBr}_3\text{Cl}_3]^{2-}$ and *trans*- $[\text{TeBr}_4\text{Cl}_2]^{2-}$ randomly distributed in the lattice [30]. The crystal structure of lithium-doped $[\text{Li}_{0.08}(\text{NH}_4)_{0.92}]_2[\text{TeBr}_2\text{Cl}_4]$ has also been inferred in terms of the disordered $[\text{TeBr}_2\text{Cl}_4]^{2-}$ anion, though no details of the disorder have been given [31]. It has recently been deduced that a reaction of TeO_2 with cesium or ammonium bromide in concentrated hydrochloric acid leads to a solid solution containing homoleptic $[\text{TeCl}_6]^{2-}$ and $[\text{TeBr}_6]^{2-}$ anions [32]. On the other hand, the Mössbauer spectra of a number of mixed hexahalogenidotellurates have been interpreted in terms of the formation of mixed anions rather than as a mixture of homoleptic anionic species [28]. The most comprehensive characterization of the mixed $[\text{TeBr}_2\text{Cl}_4]^{2-}$ and $[\text{TeBr}_4\text{Cl}_2]^{2-}$ anions is based on their vibrational spectra [24, 25, 30] combined with force-field calculations [24, 25], which has also facilitated the identification of actual isomers of the $[\text{TeBr}_x\text{Cl}_{6-x}]^{2-}$ anions.

In this work we report the characterization of homoleptic $(\text{bdmim})_2[\text{TeX}_6]$ [(bdmim = 1-butyl-2,3-dimethylimidazolium; X = Cl(**1**), Br(**2**)), as well as mixed $(\text{bdmim})_2[\text{TeBr}_2\text{Cl}_4]$ (**3**) and $(\text{bdmim})_2[\text{TeBr}_4\text{Cl}_2]$ (**4**) by using combined information from single crystal and powder X-ray crystallography, Raman spectroscopy, and solid-state DFT calculations employing periodic boundary conditions. In the case of mixed $[\text{TeBr}_2\text{Cl}_4]^{2-}$ and $[\text{TeBr}_4\text{Cl}_2]^{2-}$ anions, the DFT calculations indicate that the disorder in the crystal structures can be resolved in terms of 80 mol % of the *cis*-isomers and 20 mol % of *trans*-isomers.

2. Experimental Section.

2.1 General Procedures

Reactions were carried out in ambient conditions. 1-butyl-2,3-dimethylimidazolium halogenides (bdmim)X (X = Cl, Br) were prepared as previously reported [33]. Imidazolium halogenides are hygroscopic solids and they were dried overnight under dynamic vacuum immediately before use. TeX₄ (X = Cl, Br) (Aldrich) were used without further purification. The elemental analyses (CHN) were carried out by standard combustion techniques using a Perkin Elmer 2400 Series II CHNS/O Elemental Analyzer.

2.2 *Raman spectroscopy*

Raman spectra of the solid samples were recorded by using a Bruker IFS-66 spectrometer equipped with a FRA-106 Raman unit and Nd:YAG laser. The spectra were recorded at room temperature with 500 scans and ca. 30% laser power.

2.3 *X-Ray Crystallography. Single-Crystal Diffraction*

Diffraction data of **1-5** were collected at 120 K on a Nonius Kappa CCD diffractometer using graphite monochromated Mo K α radiation ($\lambda = 0.71073$ Å). Crystal data and the details of the structure determination are given in Table 1.

(Table 1 here)

The structures were solved using SIR-92 [34] and refined using SHELXL-97 [35]. After the full-matrix least-squares refinement of the non-hydrogen atoms with anisotropic thermal parameters, the hydrogen atoms were placed in calculated positions in the aromatic ring (0.95 Å), methyl groups (0.98 Å) and methylene groups (0.99 Å). In the final refinement, hydrogen atoms were treated using a riding model in which the isotropic thermal parameters of the hydrogen atoms are proportional to those of the carbon atoms to which they are bonded. The isotropic thermal

parameters of the aromatic and methylene hydrogen atoms were fixed at 1.2 times, and the methyl hydrogen atoms were fixed at 1.5 times to those of the corresponding carbon atoms. The scattering factors for the neutral atoms were those incorporated with the programs.

The anions of $(\text{bdmim})_2[\text{TeBr}_2\text{Cl}_4]$ (**3**) and $(\text{bdmim})_2[\text{TeBr}_4\text{Cl}_2]$ (**4**) are disordered with the halogen atom positions statistically distributed over the atomic sites. Therefore, the site occupation factors of chlorine and bromine were refined along with positional and displacement parameters. Because of the correlation between the thermal parameters and the occupation factors, the anisotropic displacement parameters of the disordered pair of atoms were constrained to be equal.

2.4 X-ray Crystallography. Powder diffraction

X-ray powder diffraction patterns of **1-4** were acquired at room temperature by a Huber Imaging Plate Guinier Diffractometer 670 in Guinier geometry (angle of incidence to the sample normal = 45°) using continuous step-scan technique with position sensitive imaging plate detector and incident beam germanium monochromator (radiation: Cu $K_{\alpha 1}$ $\lambda = 1.5406 \text{ \AA}$; 45kV and 25 mA). Each sample was prepared on a thin film (Mylar) using petrolatum jelly as an adhesive and the data were recorded using 2Θ range of $4-100^\circ$ with recording time of 60 min and step resolution of 0.005° . In order to evaluate the structural consistency between a bulk powder and the single crystals subjected to structure analysis, peak indexing of the diffraction patterns were made using Pawley fitting method [36] in program DASH 3.2 [37]. Truncated data range of $6-45^\circ$ and the unit cell settings of the corresponding single crystal structure were used as a starting point for the refinement of each pattern.

2.5 Syntheses of $(\text{bdmim})_2[\text{TeX}_6]$ [$X = \text{Cl}$ (1), Br (2)]

(bdmim)₂[TeCl₆] (**1**) was prepared by adding 0.431 g (1.60 mmol) of TeCl₄ to the CH₂Cl₂ (30 mL) solution of (bdmim)Cl (0.604 g, 3.20 mmol). The mixture was refluxed for 4.5 h and the solution was concentrated. The isolated precipitate was washed twice with CH₂Cl₂ (5 mL). Yield 0.994 g (96 %). Crystallization from MeCN afforded crystals of (bdmim)₂[TeCl₆]. Anal. Calcd. for C₁₈H₃₄N₄Cl₆Te (**1**): C 33.43 H 5.30 N 8.66. Found: C 33.35 H 5.16 N 8.46.

(bdmim)₂[TeBr₆] (**2**) was prepared in a similar fashion by refluxing a mixture of 0.748 g (3.20 mmol) of (bdmim)Br and 0.712 g (1.60 mmol) of TeBr₄ in 30 mL of CH₂Cl₂ for 4 h. The workup yielded an orange precipitate, which was washed twice with CH₂Cl₂ (7 mL). Yield 1.439 g (98 %). Crystallization from MeCN yielded orange-red crystals of (bdmim)₂[TeBr₆] together with a very small amount of yellow crystals that were identified by X-ray diffraction as (bdmim)₂[Te₂Br₁₀] (**5**). Anal. Calcd. for C₁₈H₃₄N₄Br₆Te (**2**): C 23.67 H 3.75 N 6.13. Found: C 23.52 H 3.94 N 5.94.

2.6 *Syntheses of (bdmim)₂[TeBr₂Cl₄] (3) and (bdmim)₂[TeBr₄Cl₂] (4)*

(bdmim)₂[TeBr₂Cl₄] (**3**) was prepared by adding 0.645 g (2.40 mmol) of TeCl₄ to the CH₂Cl₂ (45 mL) solution of (bdmim)Br (1.116 g, 4.80 mmol) and refluxing the mixture for 2 h. The solution was concentrated and the isolated precipitate was washed twice with CH₂Cl₂ (10 mL). Yield of **3** 1.522 g, (86 %). Crystallization from MeCN yielded orange-yellow crystals. Anal. Calcd. for C₁₈H₃₄N₄Br₂Cl₄Te (**3**): C 29.39 H 4.66 N 7.62. Found: C 29.25 H 4.63 N 7.59.

The related synthesis of (bdmim)₂Cl (0.605 g, 3.20 mmol) with TeBr₄ (0.719 g, 1.60 mmol) afforded 1.259 g (95 %) of (bdmim)₂[TeBr₄Cl₂]. Crystallization from MeCN yielded orange-yellow crystals. Anal. Calcd. for C₁₈H₃₄N₄Br₄Cl₂Te (**4**): C 26.22 H 4.16 N 6.79. Found: C 26.31 H 4.01 N 6.83.

3. Computational Details

Gas phase optimizations of all isomers of different $[\text{TeX}_n\text{Y}_{6-n}]^{2-}$ ($X = \text{Cl}$, $Y = \text{Br}$) anions were carried out using the PBE0 density functional [38-41] and correlation consistent basis sets of triple- ζ -valence quality (aug-cc-pVTZ for Cl and Br, and aug-cc-pVTZ-PP for Te) [42-44]. The optimized Cartesian coordinates of the atoms in all $[\text{TeBr}_x\text{Cl}_{6-x}]^{2-}$ ($x = 0-6$) anions are given in Supporting Information in the form of xyz-files. Frequency calculations were performed for all stationary points to ensure that the ions are minima on the potential energy surface and to calculate their IR and Raman spectra. The calculations were performed with the Gaussian 09 program package [45].

Solid state DFT calculations on **1-4** were carried out using the PBE0 functional and localized atomic basis sets composed of Gaussian-type functions. All calculations were performed with the CRYSTAL09 software package [46, 47]. The X-ray structures were used as starting points in the structural optimizations. The ordered *cis*- and *trans*-models of **3** and **4** were derived from the disordered X-ray structures in accordance with the observed site occupancies. For all structures, the atomic positions were fully optimized while the lattice parameters were kept at the experimentally observed values (see Supporting Information for optimized fractional coordinates). The Karlsruhe triple- ζ - valence + polarization basis set was applied for Te, Br, and Cl atoms [48, 49], while the counterions were described using split-valence + polarization (SVP) basis sets (see Supporting Information for basis set details). Monkhorst-Pack-type grids of k -points in the reciprocal space were generated using a shrinking factor (SHRINK) of 2 [50]. For

the evaluation of the Coulomb and exchange integrals (TOLINTEG), tight tolerance factors of 8, 8, 8, and 16 were used. Default optimization convergence thresholds and an extra-large integration grid for the density-functional part were applied in all calculations (XLGRID). The Raman frequencies were obtained by using the computational scheme implemented in CRYSTAL09 [51, 52]. The atomic masses, which were used for the calculations, were those of the most abundant isotopes in the case of each element.

4. Results and Discussion

4.1 General

Hexahalogenidotellurate(2-) anions can generally be prepared by the reaction of halogenide ions with tellurium tetrahalogenides [21, 22]. We treated two equivalents of 1-butyl-2,3-dimethylimidazolium chloride (bdmim)Cl and bromide (bdmim)Br with one equivalent of tellurium tetrachloride and -bromide, respectively, to yield (bdmim)₂[TeX₆] [X = Cl (**1**), Br (**2**)] in excellent yields. (bdmim)X was chosen as a starting material in order to have an unsymmetrical cation together with homoleptic octahedral [TeX₆]²⁻ anions.

The related reactions of (bdmim)Br with TeCl₄ and (bdmim)Cl with TeBr₄ afford salts containing mixed bromidochloridotellurate anions (bdmim)₂[TeBr₂Cl₄] (**3**) and (bdmim)₂[TeBr₄Cl₂] (**4**).

4.2 Crystal Structures

The structures of (bdmim)₂[TeX₆] [X = Cl (**1**), Br (**2**)], (bdmim)₂[TeBr₂Cl₄] (**3**), and (bdmim)₂[TeBr₄Cl₂] (**4**) are shown in Figure 1 together with the numbering of the atoms. Selected bond lengths are shown in Table 2.

(Figure 1 here)

(Table 2 here)

All lattices of **1-4** consist of discrete $[\text{TeX}_6]^{2-}$ anions and $(\text{bdmim})^+$ cations. The asymmetric units of all compounds are composed of one cation and half of the anion. Interestingly, **2-4**, which are mutually isomorphic, are also almost isomorphic with **1**. The packing of the anions in all four salts is virtually the same, but the packing of the $(\text{bdmim})^+$ cations in **1** differs from that in **2-4** (see Figures 1 and 2).

(Figure 2 here)

4.2.1 $(\text{bdmim})_2[\text{TeX}_6]$ [$X = \text{Cl}$ (**1**), Br (**2**)]

The coordination environment of tellurium in the homoleptic $[\text{TeCl}_6]^{2-}$ and $[\text{TeBr}_6]^{2-}$ anions of **1** and **2** is expectedly nearly octahedral. The X-Te-X bond angles span a narrow range of 88.72(4) - 91.28(4)° and 88.19(2) - 91.81(2)° for $[\text{TeCl}_6]^{2-}$ and $[\text{TeBr}_6]^{2-}$, respectively. The respective Te-Cl and Te-Br bond lengths of 2.5241(9)-2.5569(11) and 2.6845(7)-2.7161(8) Å in **1** and **2** are longer than the single bond lengths (2.36 and 2.51 Å, respectively [53]) but quite typical for the octahedral $[\text{TeX}_6]^{2-}$ anions. The observed regular octahedral geometry in the seven electron pair AX_6E anions have been attributed to the presence of the tellurium lone pair in the stereochemically inactive 5s orbital [54-56]. The observed long bonds can then be rationalized as 3c-4e bonds in which only the tellurium 5p orbitals participate. There is, however, significant variation in the bond lengths of the $[\text{TeX}_6]^{2-}$ salts for which the crystal structure is known. The Te-Cl distances range 2.38-2.78 Å [average 2.54(7) Å; median 2.53 Å], and those for the $[\text{TeBr}_6]^{2-}$ salts range 2.55-2.91 Å [average 2.70(6) Å; median 2.70 Å] [23]. The longest outliers

and the largest deviations from the octahedral symmetry of the anions have been associated with the presence of a hydrogen bonding network [57, 58]. The current anions of **1** and **2** show almost regular octahedral geometry with each halogen atom participating only in a very weak hydrogen bonding network between the anions and the cations. The Cl \cdots H contacts in **1** and the H \cdots Br contacts in **2** span the range 2.708(1)-2.975(1) and 2.748(6)-2.993(6) Å, respectively.

A very small amount of (bdmim)₂[Te₂Br₁₀] (**5**) was observed in the reaction product containing mainly (bdmim)₂[TeBr₆]. The crystal structure together with the numbering of atoms is shown in Figure 3 together with selected bond lengths and angles. The terminal Te-Br bond lengths span a range of 2.5430(12)-2.6944(13) Å and the bridging Te-Br distances are 2.8920(16) and 2.9862(12) Å. There is a clear *trans*-influence in the bond lengths. The terminal bonds Te1-Br3 and Te1-Br4, which are in *trans*-position to the weaker bridging bonds [Te1-Br5 and Te1-Br5^a; for the symmetry operation *a*, see Figure 3], are shorter than the terminal bonds Te1-Br1 and Te1-Br2, which are mutually in *trans*-positions.

(Figure 3 here)

The bond parameters agree well with those in other related salts of [Te₂Br₁₀]²⁻ [59-63].

4.2.2 (bdmim)₂[TeBr₂Cl₄] (**3**) and (bdmim)₂[TeBr₄Cl₂] (**4**)

Two of the three halogen atom sites in the anion of **3** and all halogen atom sites in the anion of **4** are disordered [see Figures 1(c) and 1(d)]. The refined site occupation factors are shown in Table S1 in Supporting Information. The positions of the disordered bromine and chlorine atoms could, however, be individually refined and resulted in reasonable Te-Br and Te-Cl distances for both **3** and **4** (see Table 2). Both salts are isomorphic with (bdmim)₂[TeBr₆] (**2**) and show similar

hydrogen bonding networks.

Because of the halogen atom disorder, single crystal X-ray structures cannot be used to deduce, whether the anions in **3** and **4** are single species, which can adopt several different orientations, or if the lattice is a solid solution of several different anionic species. It can, however, be inferred from the variation in the site occupation factors of bromine and chlorine (see Table S1 in Supporting Information) that these phases cannot be solid solutions of $[\text{TeBr}_6]^{2-}$ and $[\text{TeCl}_6]^{2-}$. The co-existence of several $[\text{TeBr}_x\text{Cl}_{6-x}]^{2-}$ anions as well as their different isomers to exhibit the respective overall compositions $[\text{TeBr}_2\text{Cl}_4]^{2-}$ and $[\text{TeBr}_4\text{Cl}_2]^{2-}$ in **3** and **4** is, however, possible. Furthermore, polycrystalline reaction products need not contain only one phase. Therefore, additional information has to be sought for.

4.3 X-Ray Powder Diffraction

The X-ray powder diffraction data were recorded for compounds **1-4** in order to confirm the homogeneity of the bulk material. This is especially important for the compounds **3** and **4** containing mixed halogenidotellurate anions. The Pawley refinement of the X-ray powder diagrams of **1**, **3**, and **4** resulted in the full indexing of the data and a good agreement between the recorded and calculated peak profiles, indicating that the powder samples of the compounds **1**, **3**, and **4** indeed constitute a single phase, as shown in Figures 4(a,c,d). The powder sample of **2** [see Figure 4(b)] can also be indexed in terms of $(\text{bdmim})_2[\text{TeBr}_6]$, with the exception of three very weak diffraction peaks observed at low 2θ range (peaks at 9.88, 13.92 and 14.61 °). These three peaks, however, match very well with the three strongest diffraction peaks in the diffraction pattern, which was calculated from the single-crystal X-ray structure of $(\text{bdmim})_2[\text{Te}_2\text{Br}_{10}]$ (**5**), the small amount of which was found in the reaction product containing mainly **2** as the main component.

(Figure 4 here)

Taking in to account the temperature difference in recording the single crystal and powder data (120 K and 293 K, respectively), the Pawley refinement of each diffraction pattern of **1-4** resulted in the unit cell parameters that are in good agreement (generally < 1 % thermal expansion of the unit cell axes) to that of determined from the corresponding single crystal data (see Table S2 in Supporting Information). Based on the power diffraction analyses, it can be deduced that each salt **1-4** is composed of a single phase. However, while **1** and **2** represent single compounds, there is a possibility that even though the overall compositions of **3** and **4** are consistent with the molecular formulae $(\text{bdmim})_2[\text{TeBr}_2\text{Cl}_4]$ and $(\text{bdmim})_2[\text{TeBr}_4\text{Cl}_2]$, respectively, they are composed of solid solutions of several different hexahalogenidotellurate anions.

4.4 Raman Spectroscopic Characterization

The chemical identity and structure of the four anions were inferred on the basis of combined information from Raman spectroscopy and DFT calculations of the fundamental vibrations both in the gaseous and solid state (A full listing of fundamental vibrations of all isomers of every $[\text{TeBr}_x\text{Cl}_{6-x}]^{2-}$ ($x = 0-6$) anion in vacuum is presented in Table S3 in Supporting Information).

The homoleptic $[\text{TeX}_6]^{2-}$ anions have an ideal octahedral symmetry (point group O_h), and the irreducible representations of the 15 fundamental vibrations are $A_{1g}+E_g+T_{2g}+2T_{1u}+T_{2u}$. The A_{1g} , E_g , and T_{2g} modes are Raman active, the two T_{1u} modes are IR active, and the T_{2u} mode is inactive. Therefore, three Raman peaks are expected for both $[\text{TeCl}_6]^{2-}$ and $[\text{TeBr}_6]^{2-}$ anions, as is indeed observed in case of both **1** and **2** (see Figure 5). The observed wavenumbers of these fundamental vibrations together with those calculated for the gaseous $[\text{TeCl}_6]^{2-}$ and $[\text{TeBr}_6]^{2-}$ ions

at the PBE0/aug-cc-pVTZ level of theory are presented in Table 3.

(Table 3 here)

(Figure 5 here)

It can be seen from Table 3 that the computed wavenumbers and intensities agree reasonably well with the Raman spectroscopic information for both $[\text{TeCl}_6]^{2-}$ and $[\text{TeBr}_6]^{2-}$, though in both cases the computed wavenumbers are systematically smaller than those of the observed Raman peaks. This systematic disagreement between the calculated and observed wavenumbers of the multiply-charged anions such as $[\text{TeX}_6]^{2-}$ have been explained to be due to their electronic instability in the gas phase [20]. The energy of HOMO is indeed positive (+0.00965 a.u.) in $[\text{TeCl}_6]^{2-}$ and only slightly negative (-0.00215 a.u.) in $[\text{TeBr}_6]^{2-}$. The reduced stability of these dianions in the gaseous state is consistent with the observation that the optimized PBE0/aug-cc-pVTZ bond lengths of 2.571 and 2.739 Å for $[\text{TeCl}_6]^{2-}$ and $[\text{TeBr}_6]^{2-}$, respectively, are somewhat longer than those obtained from crystal structure determinations (see Table 2).

As seen from Figure 5(a), the Raman peak at 255 cm^{-1} exhibits a shoulder at 245 cm^{-1} . In the crystal of the space group $P2_1/c$, the gas phase symmetry of O_h of the $[\text{TeX}_6]^{2-}$ ions is lowered to the site symmetry of C_{2h} . Due to the lowered site symmetry, the degeneracy of the two-dimensional E_g mode is lifted and the corresponding Raman peak is split. The corresponding splitting of the T_{2g} mode at 133 cm^{-1} is seen as a broadened peak. The two shoulders which are seen in Raman spectrum at 110 and 92 cm^{-1} are probably due to lattice vibrations. The similar lowering of site symmetry is also seen in the Raman spectrum of $[\text{TeBr}_6]^{2-}$ [see Figure 5(b)], though in this case the splittings of both the E_g and T_{2g} modes exhibit only broadened peaks.

Because of the gas-state instability and the lowering of the site symmetry, the computation of fundamental vibrations to assist the assignment of the solid state Raman spectra of **1-4** were carried out in the crystalline state at PBE0/TZVP level of theory employing periodic boundary conditions. The geometry optimization resulted in a good agreement between the calculated and observed unit cell parameters and metrical bond parameters (The difference between the calculated and observed bond lengths in both $[\text{TeCl}_6]^{2-}$ and $[\text{TeBr}_6]^{2-}$ is less than 1 %). As seen from Table 3, the fundamental vibrations calculated for the crystal structures of **1** and **2** are in much better agreement with the observed Raman lines than the values calculated for the anions in vacuum. Raman intensities could unfortunately not be obtained from the solid-state calculations. It can, however, be concluded that Raman spectroscopic information coupled with both gas phase and crystalline phase DFT calculations serves well in the characterization of the homoleptic anions $[\text{TeCl}_6]^{2-}$ and $[\text{TeBr}_6]^{2-}$.

The application of Raman spectroscopy for the identification of the anionic species in **3** and **4** is more critical, because due to disorder the presence of individual anions cannot be inferred by X-ray diffraction. As discussed above, while the elemental analyses of **3** and **4** indicate that the anions have the respective compositions of $[\text{TeBr}_2\text{Cl}_4]^{2-}$ and $[\text{TeBr}_4\text{Cl}_2]^{2-}$ and the X-ray powder diffraction data indicated the presence of only one phase in the case of both products, it is possible that several different $[\text{TeBr}_x\text{Cl}_{6-x}]^{2-}$ anions form solid solutions. This should, however, be seen in the Raman spectra of **3** and **4** by the presence of several shoulders or even close-lying discrete Raman lines in the regions of both stretching and deformation vibrations (see Table S3 in Supporting Information). The Raman spectra of neither **3** nor **4** indicate the presence of several different anionic species, as shown in Figure 6.

(Figure 6 here)

There are two possible isomers in case of both $[\text{TeBr}_2\text{Cl}_4]^{2-}$ and $[\text{TeBr}_4\text{Cl}_2]^{2-}$: *cis*- $[\text{TeX}_2\text{Y}_4]^{2-}$ (C_{2v}) and *trans*- $[\text{TeX}_2\text{Y}_4]^{2-}$ (D_{4h}). All 15 fundamental vibrations are Raman-active in the former case ($6A_1+2A_2+3B_1+4B_2$). In the latter isomer, six fundamental vibrations are Raman-active ($2A_{1g}+B_{1g}+B_{2g}+E_g$). The fundamental vibrations of the *cis*- and *trans*-isomers of $[\text{TeBr}_2\text{Cl}_4]^{2-}$ and $[\text{TeBr}_4\text{Cl}_2]^{2-}$ have been computed for the optimized geometries both in the gaseous state and in the crystalline lattice, as shown in Tables 4 and 5. Because of the electronic instability of the dianions [20], the Te-Cl and Te-Br bond lengths in both *cis*- and *trans*-isomers of $[\text{TeBr}_2\text{Cl}_4]^{2-}$ and $[\text{TeBr}_4\text{Cl}_2]^{2-}$ in the gaseous state are somewhat longer than what is expected experimentally based on the crystal structures of $[\text{TeCl}_6]^{2-}$ and $[\text{TeBr}_6]^{2-}$. The solid-state DFT optimization, however, reproduced well the experimental bond lengths (the difference between the optimized and experimental bond lengths is *ca.* 1.3 %). Consequently, while the vacuum wavenumbers show systematically too small values, the fundamental vibrations in the crystalline state seem to be in good agreement with the observed Raman wavenumbers (see Tables 4 and 5) and enable the inference of the presence of *cis*- $[\text{TeBr}_2\text{Cl}_4]^{2-}$ and *cis*- $[\text{TeBr}_4\text{Cl}_2]^{2-}$ in **3** and **4**, respectively, as described below.

(Table 4 here)

(Table 5 here)

It can be seen from Tables 4 and 5 that the observation of strong Raman lines at 178 in **3** and 174 cm^{-1} in **4** verifies the presence of the *cis*-isomers, since the *trans*-isomers are not expected to exhibit Raman lines in the wavenumber region 160-180 cm^{-1} . The A_{2u} mode in **3** calculated at 190 cm^{-1} and the E_u mode of **4** calculated at 186 cm^{-1} are both Raman inactive in the point group D_{4h} . It is, however, not possible to rule out the presence of the *trans*-isomers of $[\text{TeBr}_2\text{Cl}_4]^{2-}$ and

$[\text{TeBr}_4\text{Cl}_2]^{2-}$ by Raman spectroscopy, since all fundamental vibrations that should be observed in the Raman spectra of *trans*- $[\text{TeBr}_2\text{Cl}_4]^{2-}$ and $[\text{TeBr}_4\text{Cl}_2]^{2-}$ coincide with the fundamental vibrations of the corresponding *cis*-isomers.

The PBE0/aug-cc-pVTZ energetics of all possible isomers of the $[\text{TeCl}_x\text{Br}_{6-x}]^{2-}$ anions are consistent with the conclusions discussed above (the total Gibbs' energies of the anions have been presented in Table S4 of Supporting Information). It is interesting to note that for the compositions $[\text{TeBr}_2\text{Cl}_4]^{2-}$, $[\text{TeBr}_3\text{Cl}_3]^{2-}$, and $[\text{TeBr}_4\text{Cl}_2]^{2-}$, which each show two different isomers, the isomer with a smaller number of homoleptic X-Te-X (X = Cl, Br) *trans*-arrangements and a larger number of heteroleptic X-Te-Y *trans*-arrangements is more stable. Thus, *cis*- $[\text{TeX}_4\text{Y}_2]$ is more stable than *trans*- $[\text{TeX}_4\text{Y}_2]$ and *fac*- $[\text{TeX}_3\text{Y}_3]$ is more stable than *mer*- $[\text{TeX}_3\text{Y}_3]$. The energy difference, though small, seems to be cumulative (see Table 6). This would render it somewhat more likely that the *cis*- $[\text{TeBr}_2\text{Cl}_4]^{2-}$ and *cis*- $[\text{TeBr}_4\text{Cl}_2]^{2-}$ are more favorable than the *trans*-isomers.

(Table 6 here)

4.5 Formation of The Mixed Anions

Whereas tellurium tetrachlorides and tetrabromides exist as tetramers in the solid state [64-66], they are likely to be monomeric in solution [67-69]. Ozin and Vander Voet [25] have suggested that in the reaction between TeX_4 and Y^- , TeX_4 acts as a Lewis acid and Y^- as a base undergoing a nucleophilic attack on tellurium.

Our DFT (PBE0/aug-cc-pVTZ) calculations have shown that the uptake of Y^- by TeX_4 to form a $[\text{TeX}_4\text{Y}]^-$ monoanion takes place without energy barrier both in the gas phase and in solution

[The solvent (dichloromethane) effects were taken into account using the PCM model as implemented in Gaussian 09. For a recent review, see ref. 70]. It has been reported that the initially formed five-coordinate square pyramidal (sp) species can undergo apical/basal ligand exchange through hemidirected and/or holodirected transition state [71]. Our analysis of the potential energy surface of the $[\text{TeCl}_4\text{Br}]^-$ monoanion shows, however, that the only viable pathway for this anion involves the holodirected trigonal bipyramidal (tbp) transition state (see Scheme 1). This process has a very low activation barrier of 33 kJ mol^{-1} in solution (24 kJ mol^{-1} in the gas phase) and the resulting sp structure with a Br ligand (atom Y) on an apical site is energetically on par with the starting isomer. The energetics of the ligand exchange in $[\text{TeBr}_4\text{Cl}]^-$ is very similar.

(Scheme 1 here)

The apical/equatorial ligand exchange in $[\text{TeX}_4\text{Y}]^-$ is therefore very rapid and each ligand has an equal probability to occupy any of the four basal and one apical position in the sp monoanion. Consequently, because all of the five ligands are nominally equivalent, any one of them has 80 % probability to occupy a basal position and 20 % probability to occupy an apical position, as shown in Scheme 1. The subsequent reaction of $[\text{TeX}_4\text{Y}]^-$ with a second halide ion Y^- leads to an 80:20 mixture of *cis*- and *trans*- $[\text{TeX}_4\text{Y}_2]^{2-}$, as shown in Scheme 2. Our calculations show that in the case of $[\text{TeCl}_4\text{Br}]^-$, the addition of second Br^- also proceeds without an energy barrier (like the first addition) both in the gas phase and in solution.

(Scheme 2 here)

5. Conclusions

Discrete mixed $[\text{TeBr}_x\text{Cl}_{6-x}]^{2-}$ anions in their disordered crystal structures have been identified by using the phases prepared by the reaction of 1-butyl-2,3-dimethylimidazolium halogenides (bdmim)X with tellurium tetrahalogenides TeX_4 (X = Cl, Br) as examples. Depending on the choice of reagents, either homoleptic $[\text{TeCl}_6]^{2-}$ or $[\text{TeBr}_6]^{2-}$, or mixed $[\text{TeBr}_2\text{Cl}_4]^{2-}$ or $[\text{TeBr}_4\text{Cl}_2]^{2-}$ anions are obtained. All products were characterized with single crystal and powder X-ray diffraction, as well as Raman spectroscopy. The interpretation of structural and spectroscopic data was assisted by high-level DFT calculations, which were performed both on gas phase species and on actual crystalline phases employing periodic boundary conditions. The computations reproduced well the structural and spectroscopic information for the homoleptic salts (bdmim) $_2$ $[\text{TeCl}_6]$ and (bdmim) $_2$ $[\text{TeBr}_6]$ and thus gave confidence in the utilization of the DFT results in the identification of the mixed bromidochloridotellurates.

The DFT modeling of the reaction of TeX_4 with Y^- (X, Y = Cl, Br) leads to the conclusion that the reactions of TeCl_4 with (bdmim)Br and that of TeBr_4 with (bdmim)Cl afford mixtures, which contain 80 mol % of *cis*- $[\text{TeX}_4\text{Y}_2]^{2-}$ and 20 mol % of *trans*- $[\text{TeX}_4\text{Y}_2]^{2-}$ in both cases.

6. Supporting Information

Crystallographic information for **1-5** (excluding tables of structure factors) have been deposited with the Cambridge Crystallographic Data Center as supplementary publication numbers CCDC 929106 - 929110, respectively. These data can be obtained free of charge from The Cambridge Crystallographic Data Centre via www.ccdc.cam.ac.uk/data_request/cif. Supporting Information

also includes refined site occupation factors of chlorine and bromine in the disordered crystal structures of **3** and **4**, unit cell parameters from Pawley refinement of powder data of **1-4**, PBE0/aug-cc-pVTZ fundamental vibrations of the $[\text{TeBr}_x\text{Cl}_{6-x}]^{2-}$ ions in vacuum, total energies of the $[\text{TeBr}_x\text{Cl}_{6-x}]^{2-}$ -isomers, CRYSTAL09 solid state calculations, and optimized atomic coordinates of $[\text{TeBr}_x\text{Cl}_{6-x}]^{2-}$ anions in the form of xyz-files.

Acknowledgments. We are grateful to Dr. Johanna Kärkkäinen for her help in the synthesis of imidazolium halogenides. Financial support from the Academy of Finland is gratefully acknowledged.

7. References

- [1] R. B. Neder, T. Proffen, Diffuse Scattering and Defect Structure Simulations, A cook book using the program DISCUS. IUCr Texts on Crystallography 11, Oxford University Press, New York, 2008.
- [2] G. Ferraris, E. Makovicky, S. Merlino, Crystallography of Modular Materials. IUCr Monographs on Crystallography 15, Oxford University press, New York, 2008.
- [3] T. R. Welberry, Diffuse Scattering and Models of Disorder, IUCr Monographs on Crystallography 16, Oxford University Press, New York, 2010.
- [4] S. van Smaalen, Incommensurate Crystallography, IUCr Monographs on Crystallography 21, Oxford University Press, New York, 2012.
- [5] Y. Zhang, Z. Li, C. Esling, J. Müller, Z. Zhao, L. Zuo, J. Appl. Crystallogr. 43 (2010) 1426-1430.
- [6] R. S. Laitinen, P. Pekonen, R.J. Suontamo, Coord. Chem. Rev. 130 (1994) 1-62, and

references therein.

- [7] P. Pekonen, Y. Hiltunen, R. S. Laitinen, J. Valkonen, *Inorg. Chem.* 30, 1991, 1874-1878.
- [8] M. Gargouri, *J. Raman Spectrosc.* 30 (1999) 61-64.
- [9] (a) R. Laitinen, N. Rautenberg, J. Steidel, R. Steudel, *Z. Anorg. Allg. Chem.* 486 (1982) 116-128.
- [10] A. Maaninen, R. S. Laitinen, T. Chivers, T. A. Pakkanen, *Inorg. Chem.* 38 (1999) 3450-3454.
- [11] D. J. Williams, D. E. Partin, F.J. Lincoln, J. Kouvetakis, M. O'Keeffe, *J. Solid State Chem.* 134 (1997) 164-169.
- [12] A. Maaninen, J. Siivari, R. J. Suontamo, J. Konu, R. S. Laitinen, T. Chivers, *Inorg. Chem.* 36 (1997) 2170-2177.
- [13] Y. Barrans, J. Gaultier, S. Bracchetti, P. Guionneau, D. Chasseau, J. M. Fabre, *Synth. Met.* 103 (1999) 2042-2043.
- [14] A. N. Cheklov, *J. Struct. Chem.* 43 (2002) 338-345.
- [15] B. Z. Chowdhry, T. J. Dines, S. Jabeen, R. Withnall, *J. Phys. Chem.* 112 (2008) 10333-10347.
- [16] A. I. Baranov, M. Kohout, *J. Comput. Chem.* 32 (2011) 2064-2076.
- [17] L. Smrcok, M. Brunelli, M. Boca, M. Kucharik, *J. Appl. Crystallogr.* 41 (2008) 634-636.
- [18] R. Baddour-Hadjean, M. B. Smirnov, K. S. Smirnov, V. Yu. Kazimirov, J. M. Gallardo-Amores, U. Amador, M. E. Arroyo-de Dompablo, J.P. Pereira-Ramos, *Inorg. Chem.* 51, (2012) 3194-3201.
- [19] D. Galimberti, C. Quarti, A. Milani, L. Brambilla, B. Civalieri, C. Castiglioni, *Vibr. Spectrosc.* 66 (2013) 83-92.
- [20] M. Gutowski, A. I. Boldyrev, J. V. Ortiz, J. Simons, *J. Am. Chem. Soc.* 116 (1994) 9262-9268.

- [21] B. Krebs, F.-P. Ahlers, *Adv. Inorg. Chem.* 35 (1990) 235–317.
- [22] Z. Wu, in F. A. Devillanova (ed.), *Handbook of Chalcogen Chemistry*, RSC Publishing, Cambridge, 2007, pp. 457–476.
- [23] ConQuest, Version 1.14, Cambridge Crystallographic Data Center, U.K., 2012. <http://www.ccdc.cam.ac.uk>.
- [24] G. A. Ozin, A. Vander Voet, *Can. J. Chem.* 49 (1971) 704–708.
- [25] G. A. Ozin, A. Vander Voet, *J. Mol. Struct.* 13 (1972) 435–457.
- [26] J. R. Masaguer, C. Rodriguez, M. V. Vazquez, *Acta Cient. Compost.* 14 (1977) 301–311.
- [27] R. C. Paul, R.-P. Sharma, R. D. Verma, *Indian J. Chem.* 15A (1977) 359–360.
- [28] N. S. Dance, P. Dobud, C. H. W. Jones, *Can. J. Chem.* 59 (1981) 913–917.
- [29] T. Schoenherr, *Inorg. Chim. Acta* 144 (1988) 151–153.
- [30] W. Abriel, H. Erhardt, *Z. Naturforsch., Teil B* 43 (1988) 557–560.
- [31] W. Ben Aribia, M. Abdelmouleh, R. Karray, A. Van Der Lee, A. Kabadou, A. Ben Salah, *J. Mol. Struct.* 986 (2011) 86–91.
- [32] H. Belgaroui, M. Loukil, R. Karray, A. Ben Salah, A. Kabadou, *J. Alloys Compd.* 499 (2010) L5–L8.
- [33] J. Kutuniva, R. Oilunkaniemi, R. S. Laitinen, J. Asikkala, J. Kärkkäinen, M. K. Lajunen, *Z. Naturforsch., Teil B* 62 (2007) 868–870.
- [34] A. Altomare, G. Cascarano, C. Giacovazzo, A. Gualardi, *J. Appl. Cryst.* 26 (1993) 343–350.
- [35] G.M. Sheldrick, *Acta Crystallogr., Sect. A* A46 (1990) 467–473; *ibid.* A64 (2008) 112–122.
- [36] G. S. Pawley, *J. Appl. Cryst.* 14 (1981) 357–361.
- [37] W.I.F. David, K. Shankland, J. van de Streek, E. Pidcock, W.D.S. Motherwell, J.C. Cole, *J. Appl. Cryst.* 39 (2006) 910–915.

- [38] J.P. Perdew, K. Burke, M. Ernzerhof, *Phys. Rev. Lett.* 77 (1996) 3865–3868.
- [39] J.P. Perdew, K. Burke, M. Ernzerhof, *Phys. Rev. Lett.* 78 (1997) 1396.
- [40] J.P. Perdew, M. Ernzerhof, K. Burke, *J. Chem. Phys.* 105 (1996) 9982–9985.
- [41] C. Adamo, V. Barone, *J. Chem. Phys.* 110 (1999) 6158–6170.
- [42] K.A. Peterson, D. Figgen, E. Goll, H. Stoll, M. Dolg, *J. Chem. Phys.* 119 (2003) 11113–11123.
- [43] A.K. Wilson, D.E. Woon, K.A. Peterson, T.H. Dunning, Jr., *J. Chem. Phys.* 110 (1999) 7667–7676.
- [44] D.E. Woon, T.H. Dunning, Jr., *J. Chem. Phys.* 98 (1993) 1358–1371.
- [45] M.J. Frisch, G.W. Trucks, H.B. Schlegel, G.E. Scuseria, M.A. Robb, J.R. Cheeseman, G. Scalmani, V. Barone, B. Mennucci, G.A. Petersson, H. Nakatsuji, M. Caricato, X. Li, H.P. Hratchian, A.F. Izmaylov, J. Bloino, G. Zheng, J.L. Sonnenberg, M. Hada, M. Ehara, K. Toyota, R. Fukuda, J. Hasegawa, M. Ishida, T. Nakajima, Y. Honda, O. Kitao, H. Nakai, T.J.A. Vreven, J. Montgomery, J.E. Peralta, F. Ogliaro, M. Bearpark, J.J. Heyd, E. Brothers, K.N. Kudin, V.N. Staroverov, T. Keith, R. Kobayashi, J. Normand, K. Raghavachari, A. Rendell, J.C. Burant, S.S. Iyengar, J. Tomasi, M. Cossi, N. Rega, J.M. Millam, M. Klene, J.E. Knox, J.B. Cross, V. Bakken, C. Adamo, J. Jaramillo, R. Gomperts, R.E. Stratmann, O. Yazyev, A.J. Austin, R. Cammi, C. Pomelli, J.W. Ochterski, R.L. Martin, K. Morokuma, V.G. Zakrzewski, G.A. Voth, P. Salvador, J.J. Dannenberg, S. Dapprich, A.D. Daniels, O. Farkas, J.B. Foresman, J.V. Ortiz, J. Cioslowski, D.J. Fox, GAUSSIAN 09, Gaussian, Inc., Wallingford, CT, 2009.
- [46] R. Dovesi, R. Orlando, B. Civalleri, C. Roetti, V. R. Saunders, C.M. Zicovich-Wilson, *Z. Kristallogr.* 220 (2005) 571–573.
- [47] R. Dovesi, V.R. Saunders, C. Roetti, R. Orlando, C.M. Zicovich-Wilson, F. Pascale, B. Civalleri, K. Doll, N.M. Harrison, I.J. Bush, P. D’Arco, M. Llunell, CRYSTAL2009. A

Computational Tool for Solid State Chemistry and Physics, User's Manual; University of Torino, Torino, 2009. <http://www.crystal.unito.it>.

- [48] A. Schäfer, C. Huber, R. Ahlrichs, *J. Chem. Phys.* 100 (1994) 5829–5835.
- [49] F. Weigend, R. Ahlrichs, *Phys. Chem. Chem. Phys.* 7 (2005) 3297–3305.
- [50] H.J. Monkhorst, J.D. Pack, *Phys. Rev. B* 13 (1976) 5188–5192.
- [51] F. Pascale, C.M. Zicovich-Wilson, F.L. Gejo, B. Civalleri, R. Orlando, R. Dovesi, *J. Comput. Chem.* 25 (2004) 888–897.
- [52] C.M. Zicovich-Wilson, F. Pascale, C. Roetti, V.R. Saunders, R. Orlando, R. Dovesi, *J. Comput. Chem.* 25 (2004) 1873–1881.
- [53] J. Emsley, *The Elements*, 3rd Ed., Clarendon Press, Oxford, 1998.
- [54] T.C. Gibb, R. Greatrex, N.N. Greenwood, A.C. Sarma, *J. Chem. Soc. A* (1970) 212–217.
- [55] B.M. Cheyne, J.J. Johnstone, C.H.W. Jones, *Chem. Phys. Lett.* 14 (1972) 545–548.
- [56] M.C. Aragoni, M. Arca, F.A. Devillanova, F. Isaia, V. Lippolis, *Cryst. Growth Des.* 12 (2012) 2769–2779.
- [57] G.R. Willey, D.R. Aris, W. Aemaeg, W. Errington, *Inorg. Chim. Acta* 317 (2001) 304–313.
- [58] L.-J. Baker, C.E.F. Rickard, M.J. Taylor, *Polyhedron* 14 (1995) 401–405.
- [59] N. Kuhn, A. Abu-Rayyan, K. Eichele, S. Schwarz, M. Steimann, *Inorg. Chim. Acta* 357 (2004) 1799–1804.
- [60] B. Krebs, K. Büscher, *Z. Anorg. Allg. Chem.* 463 (1980) 56–64.
- [61] S. Hauge, V. Janickis, K. Maroy, *Acta Chem. Scand.* 53 (1999) 992–996.
- [62] S.M. Närhi, R. Oilunkaniemi, R.S. Laitinen, M.A. Ahlgrén, *Inorg. Chem.* 43 (2004) 3742–3750.
- [63] A. Hammerschmidt, S. Bonmann, M. Läge, B. Krebs, *Z. Anorg. Allg. Chem.* 630 (2004) 2035–2041.

- [64] B. Buss, B. Krebs, *Inorg. Chem.*, 10 (1971) 2795–2800.
- [65] B. Buss, B. Krebs, *Angew. Chem.*, 82 (1970) 446–447.
- [66] C.B. Shoemaker, S.C. Abrahams, *Acta Crystallogr*, 18 (1965) 296.
- [67] D. M. Adams, P. J. Lock, *J. Chem. Soc. A*, (1967) 145–147.
- [68] I. R. Beattie, H. Chudzynska, *J. Chem. Soc. A*, (1967) 984–990.
- [69] N. Katsaros, J. W. George, *Inorg. Chem. Acta* 3 (1969) 165-167.
- [70] J. Tomasi, B. Mennucci, R. Cammi, *Chem. Rev.* 105 (2005) 2999-3093.
- [71] H.S. Rzepa, M.E. Cass, *Inorg. Chem.* 45 (2006) 3958-3963.

Figure Captions

Figure 1. Crystal structures together with the numbering of the atoms of (a) $(\text{bdmim})_2[\text{TeCl}_6]$ (**1**), (b) $(\text{bdmim})_2[\text{TeBr}_6]$ (**2**), (c) $(\text{bdmim})_2[\text{TeBr}_2\text{Cl}_4]$ (**3**), and (d) $(\text{bdmim})_2[\text{TeBr}_4\text{Cl}_2]$ (**4**). The thermal ellipsoids have been drawn at 50 % probability level.

Figure 2. The packing of ions in the crystal structure of (a) $(\text{bdmim})_2[\text{TeCl}_6]$ (**1**) and (b) $(\text{bdmim})_2[\text{TeBr}_6]$ (**2**), which is isomorphic with $(\text{bdmim})_2[\text{TeBr}_2\text{Cl}_4]$ (**3**) and $(\text{bdmim})_2[\text{TeBr}_4\text{Cl}_2]$ (**4**).

Figure 3. Crystal structure of $(\text{bdmim})_2[\text{Te}_2\text{Br}_{10}]$ (**5**) indicating the numbering of the atoms. The thermal ellipsoids have been drawn at 50 % probability level. Selected bond lengths (Å) and angles (°): Te1-Br1 2.6944(13), Te1-Br2 2.6758(13), Te1-Br3 2.5705(14), Te1-Br4 2.5430(12), Te1-Br5 2.8920(16), Te1-Br5^a 2.9862(12); Br1-Te1-Br2 176.15(4), Br1-Te1-Br3 90.45(4), Br1-Te1-Br4 86.83(4), Br1-Te1-Br5 91.96(4), Br1-Te1-Br5^a 91.23(4), Br2-Te1-Br3 89.89(4), Br2-Te1-Br4 89.33(4), Br2-Te1-Br5 88.22(4), Br2-Te1-Br5^a 92.61(3), Br3-Te1-Br4 93.33(4), Br3-Te1-Br5 171.99(4), Br3-Te1-Br5^a 87.05(4), Br4-Te1-Br5 94.43(4), Br4-Te1-Br5^a 178.02(4), Br5-Te1-Br5^a 85.26(4), Te1-Br5-Te1^a 94.74(4). The symmetry operation *a*: -*x*, -*y*, -*z*.

Figure 4. Observed and calculated X-ray powder diffraction patterns of (a) $(\text{bdmim})_2[\text{TeCl}_6]$ (**1**), $(\text{bdmim})_2[\text{TeBr}_6]$ (**2**), $(\text{bdmim})_2[\text{TeBr}_2\text{Cl}_4]$ (**3**), and $(\text{bdmim})_2[\text{TeBr}_4\text{Cl}_2]$ (**4**). The three very weak diffraction peaks indicated with a ‘ ’ can be indexed in terms of $(\text{bdmim})_2[\text{Te}_2\text{Br}_{10}]$ (**5**).

Figure 5. Raman spectra of (a) $(\text{bdmim})_2[\text{TeCl}_6]$ (**1**) and (b) $(\text{bdmim})_2[\text{TeBr}_6]$ (**2**) displayed in the region of the fundamental vibrations of the $[\text{TeX}_6]^{2-}$ anion.

Figure 6. Raman spectra of (a) $(\text{bdmim})_2[\text{TeBr}_2\text{Cl}_4]$ (**3**) and (b) $(\text{bdmim})_2[\text{TeBr}_4\text{Cl}_2]$ (**4**) recorded at room temperature.

Schemes

Scheme 1. The formation of square pyramidal $[\text{TeX}_4\text{Y}]^-$ monoanion and the apical/basal ligand exchange through holodirected trigonal bipyramidal transition state.

Scheme 2. The formation of *cis*- and *trans*- $[\text{TeX}_4\text{Y}_2]^{2-}$ from the different isomers of $[\text{TeX}_4\text{Y}]^-$.

Table 1. Details of the structure determination of (bdmim)₂[TeCl₆] (**1**), (bdmim)₂[TeBr₆] (**2**), (bdmim)₂[TeBr₂Cl₄] (**3**), (bdmim)₂[TeBr₄Cl₂] (**4**), and (bdmim)₂[Te₂Br₁₀] (**5**).^a

	1	2	3	4	5
Formula	C ₁₈ H ₃₄ N ₄ Cl ₆ Te	C ₁₈ H ₃₄ N ₄ Br ₆ Te	C ₁₈ H ₃₄ N ₄ Br _{1.68} Cl _{4.32} Te	C ₁₈ H ₃₄ N ₄ Br _{4.32} Cl _{1.68} Te	C ₁₈ H ₃₄ N ₄ Br ₁₀ Te ₂
Fw	646.80	913.55	724.13 ^b	837.84 ^b	1360.79
crystal system	monoclinic	monoclinic	monoclinic	monoclinic	monoclinic
space group	<i>P</i> 2 ₁ / <i>c</i>	<i>P</i> 2 ₁ / <i>c</i>	<i>P</i> 2 ₁ / <i>c</i>	<i>P</i> 2 ₁ / <i>c</i>	<i>P</i> 2 ₁ / <i>n</i>
<i>a</i> , Å	10.527(2)	10.553(2)	10.323(2)	10.444(2)	10.662(2)
<i>b</i> , Å	12.968(3)	14.037(3)	13.938(3)	13.995(3)	15.482(3)
<i>c</i> , Å	10.535(2)	10.763(2)	10.623(2)	10.708(2)	12.086(2)
β, deg	112.32(3)	117.72(3)	117.39(3)	117.58(3)	115.67(3)
<i>V</i>	1330.4(5)	1411.4(5)	1357.1(5)	1387.4(5)	1798.1(6)
<i>Z</i>	2	2	2	2	2
ρ _{calcd} , g cm ⁻³	1.615	2.150	1.772 ^b	2.006 ^b	2.513
μ(MoKα), mm ⁻¹	1.734	9.560	4.090 ^b	7.439 ^b	12.750
<i>F</i> (000)	648	864	710.6 ^b	802.7 ^b	1248
crystal size (mm ³)	0.30×0.15×0.10	0.20×0.20×0.20	0.15×0.10×0.08	0.20×0.15×0.15	0.30×0.15×0.10
θ range (°)	2.61 - 26.00	3.61 - 25.00	2.92 - 26.00	3.62 - 26.00	2.51 - 25.00
reflns collected	9811	9411	10665	9997	10414
unique reflns	2591	2380	2621	2705	3088
<i>R</i> _{int}	0.0850	0.0944	0.0620	0.0744	0.1060
<i>R</i> ₁ ^c	0.0448	0.0532	0.0338	0.0335	0.0705
<i>wR</i> ₂ ^d	0.1278	0.1425	0.0908	0.0779	0.2079
GOF on <i>F</i> ²	1.030	1.141	1.019	1.031	1.034

^a *T* = 120(2) K. ^b The formulae and some crystal data of **3** and **4** are based on the sums of the refined site occupation factors. ^c *R*₁ = [Σ||*F*_o| - |*F*_c||]/[Σ|*F*_o|] [*I* > 2σ(*I*)]. ^d *wR*₂ = {[Σ*w*(*F*_o² - *F*_c²)²]/[Σ*w*(*F*_o²)²]}^{1/2} [all data].

Table 2. Tellurium-halogen bond lengths (Å) in (bdmim)₂[TeCl₆] (**1**), (bdmim)₂[TeBr₆] (**2**), (bdmim)₂[TeBr₂Cl₄] (**3**), and (bdmim)₂[TeBr₄Cl₂] (**4**).

Bond	1	2	3	4
Te1-Cl1	2.5351(9)		2.5641(9)	2.539(8)
Te1-Cl2	2.5569(11)		2.572(8)	2.551(10)
Te1-Cl3	2.5241(9)		2.558(8)	2.541(10)
Te1-Br1		2.6845(7)		2.673(4)
Te1-Br2		2.7161(8)	2.714(4)	2.7151(9)
Te1-Br3		2.7083(9)	2.709(5)	2.7095(11)

Table 3. The observed Raman wavenumbers and the calculated Raman-active fundamental vibrations of $[\text{TeCl}_6]^{2-}$ and $[\text{TeBr}_6]^{2-}$ (in cm^{-1}).

$[\text{TeCl}_6]^{2-}$				$[\text{TeBr}_6]^{2-}$				
Obs1 ^a	Obs2 ^b	Obs3 ^c	DFT(g) ^{a,d}	DFT(c) ^{a,e}	Obs1 ^a	Obs2 ^b	DFT(g) ^{a,d}	DFT(c) ^{a,e}
288 s	300	287	270 (47) A_{1g}	300 A_g	173 s	180	164 (38)	182 A_g
255 s	251	247	219 (30) E_g	250 A_g	153 s	154	137 (21)	156, 149 A_g+A_g
245 sh				238 A_g	91 w ^f	90	70 (7)	95 B_g
133 s	141	131	111 (9) T_{2g}	143 B_g				89 B_g
110 sh				141 B_g				86 A_g
92 sh ^f				139 A_g				

^a This work. ^b Ref. 10g. ^c Ref. 26b. ^d Single species in the gaseous state. Molecular symmetry O_h ; PBE0/aug-cc-pVTZ level of theory. ^e Anion in the crystal structure. Site symmetry C_{2h} ; PBE0/TZVP level of theory. ^f Attenuated by the Rayleigh-line filter.

Table 4. The observed Raman wavenumbers and the calculated Raman-active fundamental vibrations of $[\text{TeBr}_2\text{Cl}_4]^{2-}$ (in cm^{-1}).

$(\text{bdmim})_2[\text{TeBr}_2\text{Cl}_4]^a$					$\text{Cs}_2[\text{TeBr}_2\text{Cl}_4]^b$	$(\text{Et}_4\text{N})_2[\text{TeBr}_2\text{Cl}_4]^b$
Raman lines	DFT(g) ^c		DFT(c) ^d		Raman lines	Raman lines
	<i>cis-</i> $[\text{TeBr}_2\text{Cl}_4]^{2-}$	<i>trans-</i> $[\text{TeBr}_2\text{Cl}_4]^{2-}$	<i>cis-</i> $[\text{TeBr}_2\text{Cl}_4]^{2-}$	<i>trans-</i> $[\text{TeBr}_2\text{Cl}_4]^{2-}$	<i>cis-</i> $[\text{TeBr}_2\text{Cl}_4]^{2-}$	<i>cis-</i> $[\text{TeBr}_2\text{Cl}_4]^{2-}$
270 <i>s</i>	262 (39) A_1	259 (41) A_{1g}	283 A	284 A_g	285 <i>s</i> A_1	282 <i>s</i> A_1
					276 <i>ms</i> B_2	
239 <i>s</i>	237 (17) B_2	223 (29) B_{1g}	264 A	249 A_g	243 <i>s</i> A_1	242 <i>s</i> A_1
	232 (<1) B_2				235 <i>ms</i> B_1	
	231 (23) A_1					
178 <i>s</i>	168 (14) A_1		188 A		186 <i>s</i> A_1	175 <i>w</i> B_2
					175 <i>m</i> B_2	
155 <i>s</i>	159 (12) B_2	139 (26) A_{1g}	176 B	156 A_g	163 <i>s</i>	
					152 <i>vw</i>	
128 <i>s</i>	115 (5) B_1	113 (8) B_{2g}	142 $B+B$	149 A_g	134 <i>s</i>	124 <i>s</i>
107 <i>sh</i>	109 (7) A_2	92 (7) E_g	97 A	124 B_g+B_g	114 <i>vw</i>	
99 <i>sh</i>	106 (4) A_1				90 <i>s</i>	
	81 (1) A_1				85 <i>m</i>	
	80 (1) B_2				65 <i>w</i>	
	75 (3) B_1				52 <i>m</i>	
	67 (<1) B_2					
	56 (1) A_2					
	54 (3) A_1					

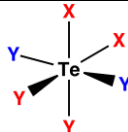
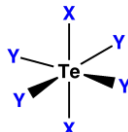
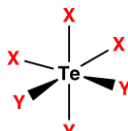
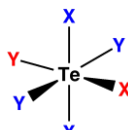
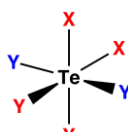
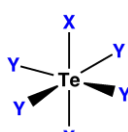
^a This work ^b Ref. 10 ^c Single species in the gaseous state. PBE0/aug-cc-pVTZ level of theory ^d Anion in the crystal structure. PBE0/TZVP level of theory.

Table 5. The observed Raman wavenumbers and the calculated Raman-active fundamental vibrations of $[\text{TeBr}_4\text{Cl}_2]^{2-}$ (in cm^{-1}).

Raman lines	$(\text{bdmim})_2[\text{TeBr}_4\text{Cl}_2]^a$		$\text{Cs}_2[\text{TeBr}_4\text{Cl}_2]^b$		
	DFT(g) ^c		DFT(c) ^d		Raman lines
	<i>cis-</i> $[\text{TeBr}_4\text{Cl}_2]^{2-}$	<i>trans-</i> $[\text{TeBr}_4\text{Cl}_2]^{2-}$	<i>cis-</i> $[\text{TeBr}_4\text{Cl}_2]^{2-}$	<i>trans-</i> $[\text{TeBr}_4\text{Cl}_2]^{2-}$	<i>cis-</i> $[\text{TeBr}_4\text{Cl}_2]^{2-}$
264 <i>s</i>	251 (28) A_1	247 (35) A_{1g}	261 <i>A</i>	261 A_g	268 <i>vw</i>
248 <i>s</i>	238 (16) B_2		242 <i>B</i>		243 <i>s</i>
232 <i>sh</i>					230 <i>sh</i>
					222 <i>s</i>
183 <i>sh</i>	185 (<1) B_1				185 <i>sh</i>
174 <i>s</i>	172 (16) A_1	150 (31) A_{1g}	182 <i>A</i>	166 A_g	173 <i>s</i>
153 <i>s</i>	158 (12) B_2				155 <i>s</i>
	140 (23) A_1	135 (22) B_{1g}	153 <i>A</i>	152 A_g	
119 <i>s</i>	106 (4) A_1	93 (6) E_g	127 <i>A</i>	127 B_g+B_g	110 <i>m</i>
97 <i>m</i>	93 (3) B_2		89 <i>B+B</i>	92 A_g	92 <i>s</i>
85 <i>m</i>	90 (4) A_2	68 (7) B_{2g}			70 <i>s</i>
	75 (<1) A_1				
	66 (2) B_2				
	62 (3) B_1				
	54 (2) B_2				
	53 (<1) A_2				
	49 (1) A_1				

^a This work ^b Ref. 10b ^c Single species in the gaseous state. PBE0/aug-cc-pVTZ level of theory ^d Anion in the crystal structure. PBE0/TZVP level of theory.

Table 6. The number of the homo- and heteronuclear *trans*-X-Te-Y arrangements and the relative energies in *cis*- and *trans*-isomers of $[\text{TeX}_2\text{Y}_4]^{2-}$ and *fac*- and *mer*-isomers of $[\text{TeX}_3\text{Y}_3]^{2-}$.

Anion		X-Te-X, Y-Te-Y	X-Te-Y	$E_{\text{rel.}}$ (kJ mol ⁻¹)
<i>cis</i> - $[\text{TeBr}_2\text{Cl}_4]^{2-}$		1	2	0.0
<i>trans</i> - $[\text{TeBr}_2\text{Cl}_4]^{2-}$		3	0	3.8
<i>fac</i> - $[\text{TeBr}_3\text{Cl}_3]^{2-}$		0	3	0.0
<i>mer</i> - $[\text{TeBr}_3\text{Cl}_3]^{2-}$		2	1	0.8
<i>cis</i> - $[\text{TeBr}_4\text{Cl}_2]^{2-}$		1	2	0.0
<i>trans</i> - $[\text{TeBr}_4\text{Cl}_2]^{2-}$		3	0	3.7

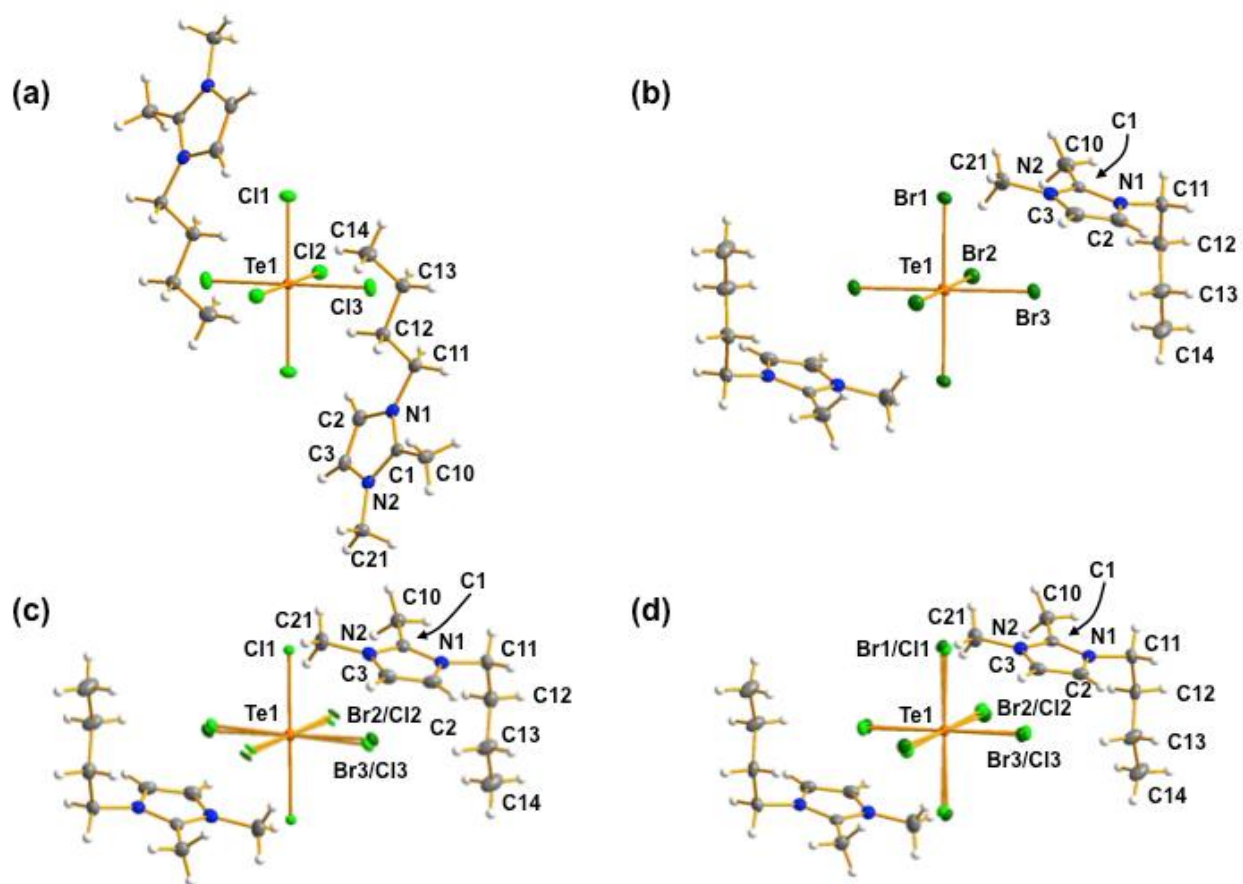


Figure 1

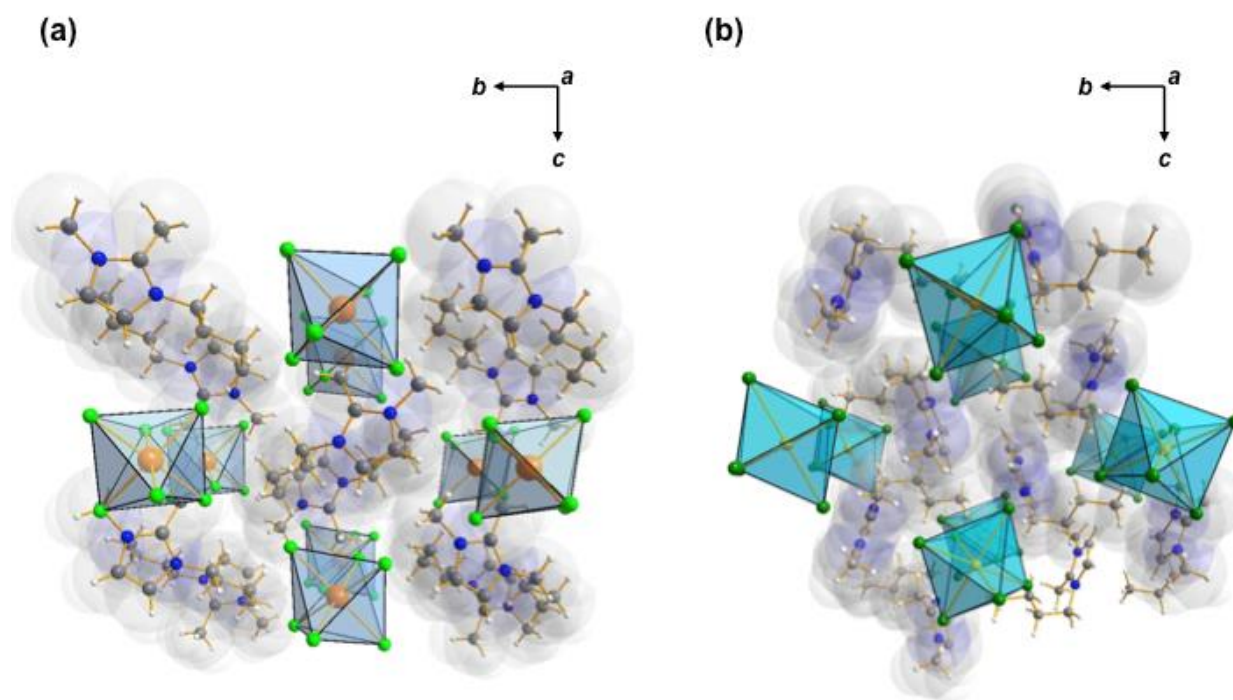


Figure 2

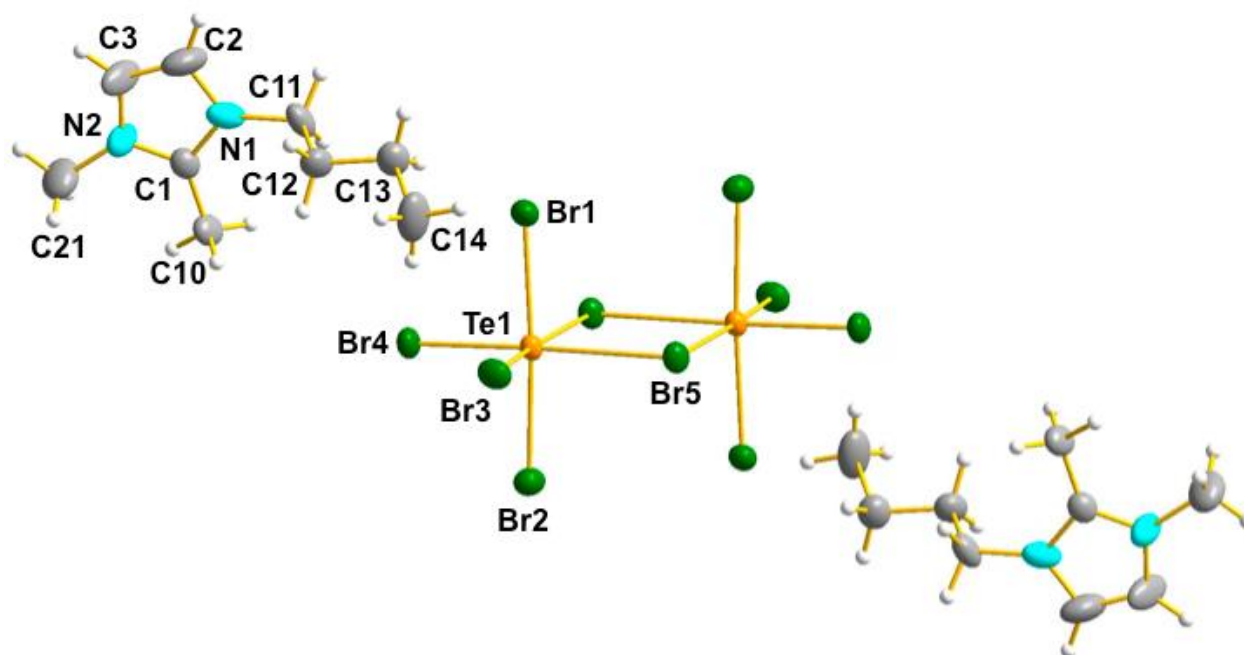


Figure 3

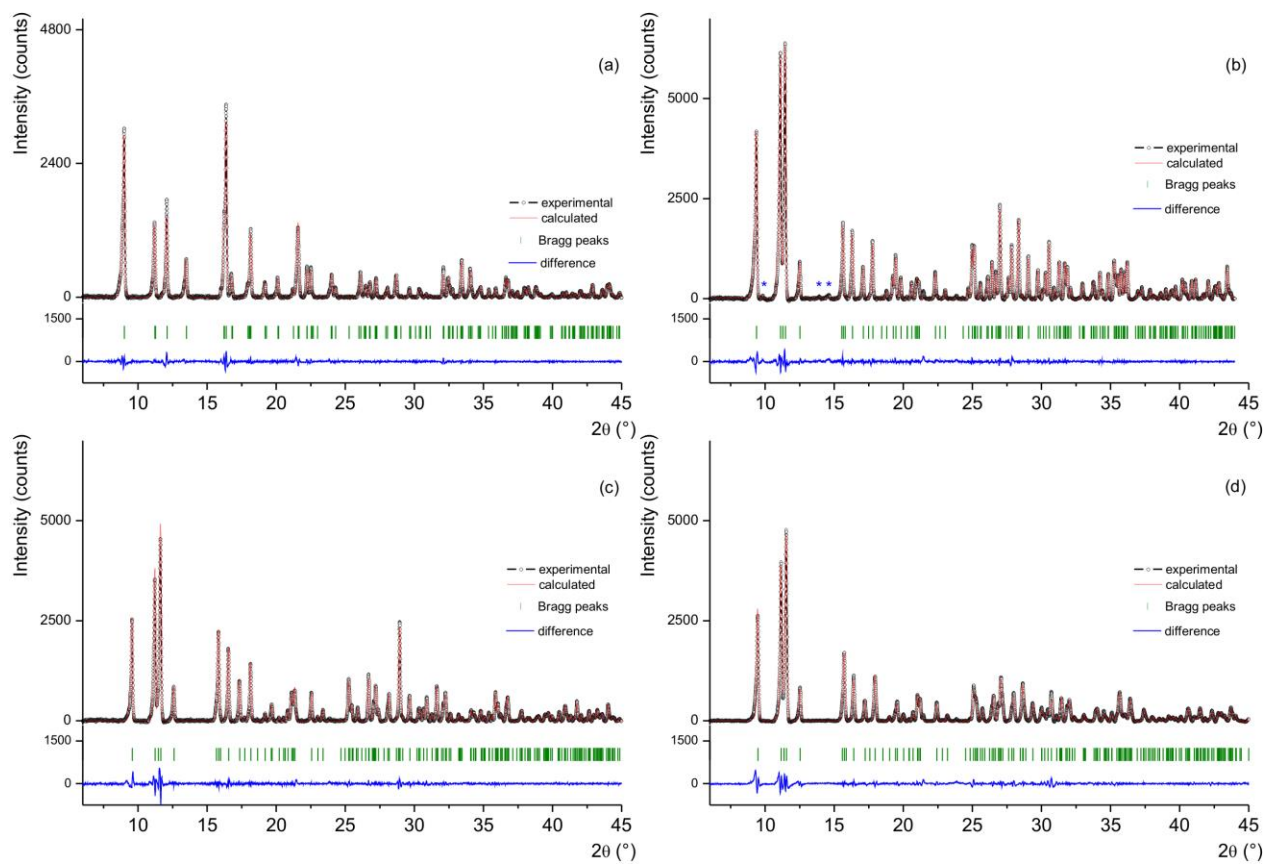


Figure 4

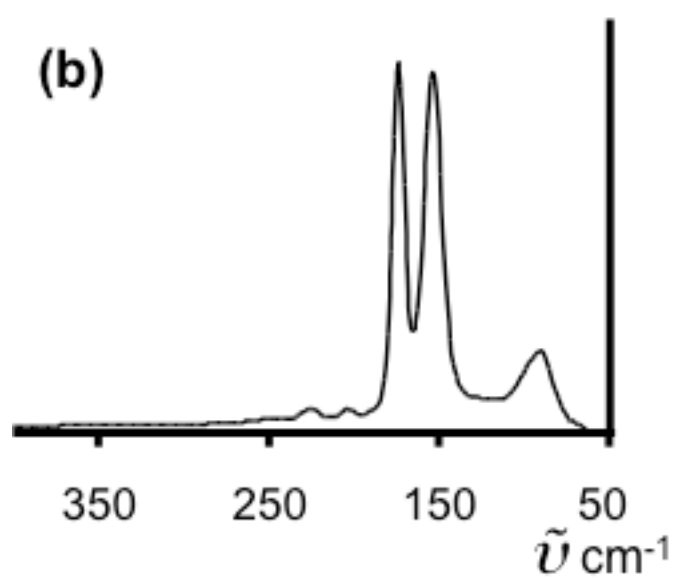
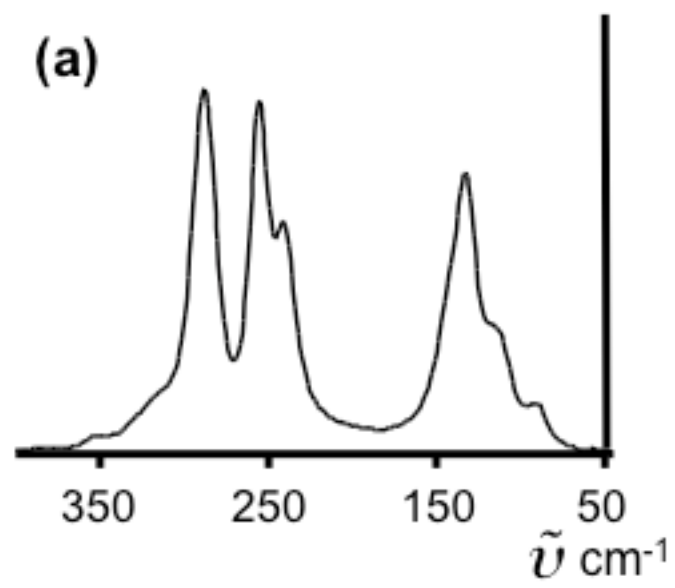


Figure 5

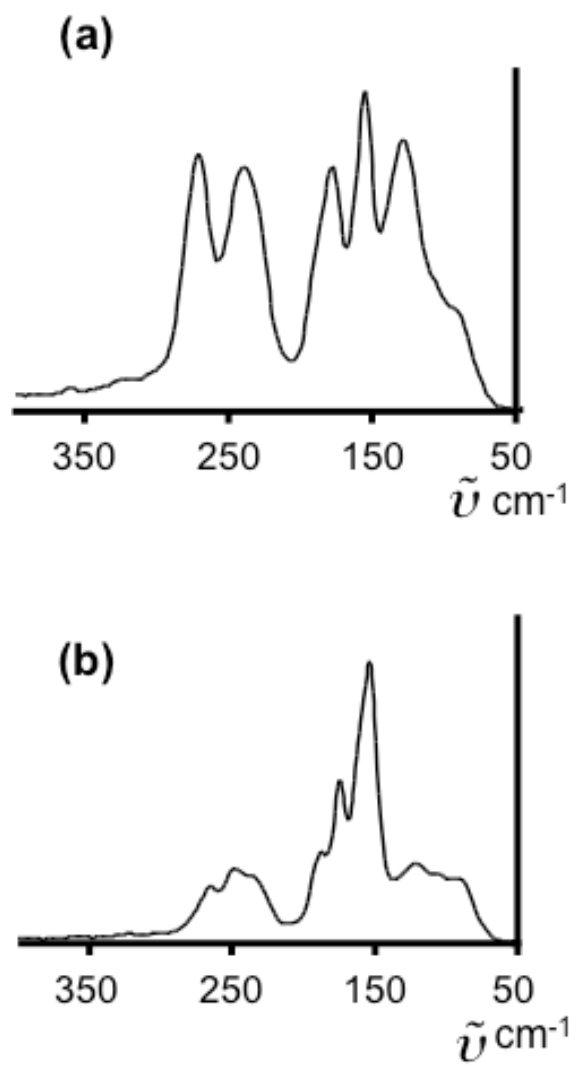
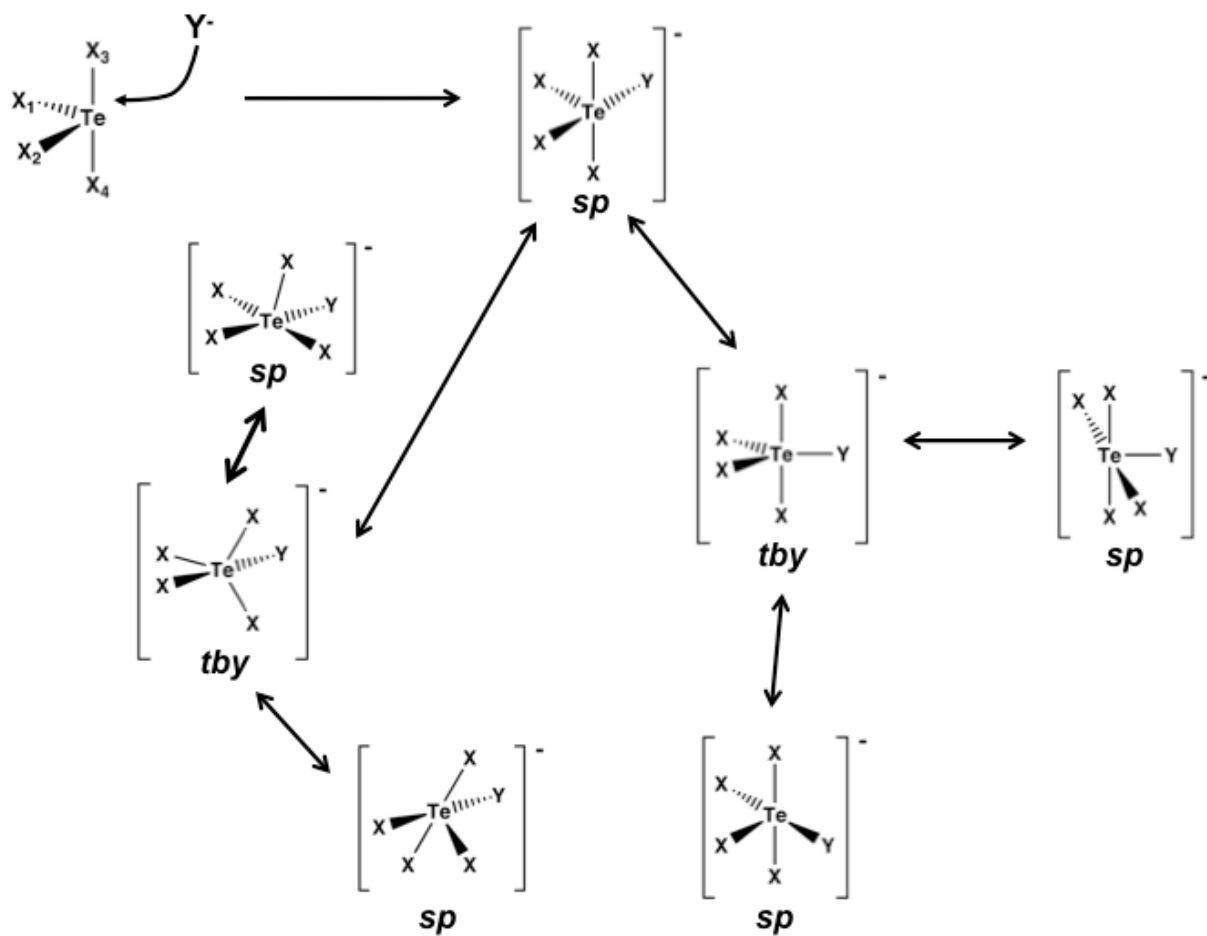
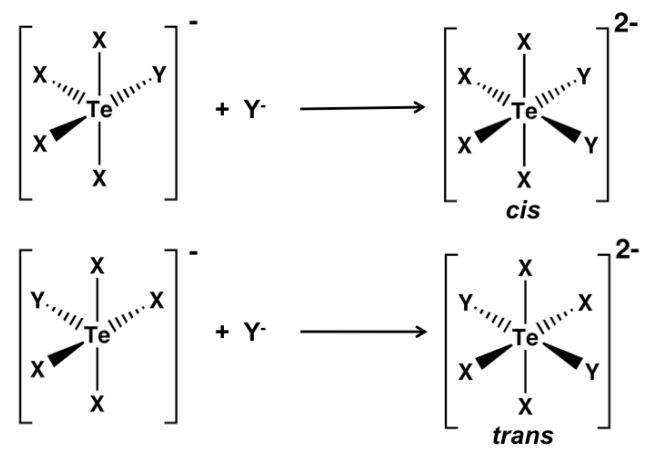


Figure 6



Scheme 1



Scheme 2